Available online at www.sciencedirect.com
ScienceDirect
Geochimica et Cosmochimica Acta 71 (2007) 71–86
Geochimica
www.elsevier.com/locate/gca

$^{228}Ra/^{226}Ra$ and $^{226}Ra/Ba$ ratios to track barite formation and transport in the water column

P. van Beek [a,*], R. François [b,1], M. Conte [b,2], J.-L. Reyss [c], M. Souhaut [a], M. Charette [b]

[a] *LEGOS, Laboratoire d'Etudes en Géophysique et Océanographie Spatiales (CNRS/CNES/IRD/UPS), Observatoire Midi Pyrénées, 14 avenue Edouard Belin, 31400 Toulouse, France*
[b] *Woods Hole Oceanographic Institution, Woods Hole, MA 02543, USA*
[c] *Laboratoire des Sciences du Climat et de l'Environnement, 91198 Gif-sur-Yvette, France*

Received 3 November 2005; accepted in revised form 12 July 2006

Abstract

We measured $^{228}Ra_{ex}/^{226}Ra_{ex}$ and $^{226}Ra_{ex}/Ba_{ex}$ ratios in suspended and sinking particles collected at the Oceanic Flux Program (OFP) time-series site in the western Sargasso Sea and compared them to seawater ratios to provide information on the origin and transport of barite ($BaSO_4$) in the water column. The $^{228}Ra_{ex}/^{226}Ra_{ex}$ ratios of the suspended particles down to 2000 m are nearly identical to those of seawater at the same water depth. These ratios are much lower than expected if suspended barite was produced in surface waters and indicate that barite is produced throughout the mesopelagic layer. The $^{228}Ra_{ex}/^{226}Ra_{ex}$ activity ratios of sinking particles collected at 1500 and 3200 m varied mostly between 0.1 and 0.2, which is intermediate between the seawater ratio at these depths (<0.03) and the seawater ratios found in the upper 250 m (0.31–0.42). This suggests that excess Ba (i.e., $Ba_{ex} = Ba_{total} - Ba_{lithogenic}$), considered to be mainly barite, present in the sinking flux is a mixture of crystals formed recently in the upper water column, formed several years earlier in the upper water column, or formed recently in deeper waters. We observe a sizeable temporal variability in the $^{228}Ra_{ex}/^{226}Ra_{ex}$ ratios of sinking particles, which indicates temporal variability in the relative proportion of barite crystals originating from surface (with a high $^{228}Ra_{ex}/^{226}Ra_{ex}$ ratio) and mesopelagic (with a low $^{228}Ra_{ex}/^{226}Ra_{ex}$ ratio) sources. However, we could not discern a clear pattern that would elucidate the factors that control this variability. The $^{226}Ra/Ba$ ratios measured in seawater are consistent with the value reported from the GEOSECS expeditions (2.3 dpm μmol^{-1}) below 500 m depth, but are significantly lower in the upper 500 m. High $^{226}Ra_{ex}/Ba_{ex}$ ratios and elevated Sr concentrations in suspended particles from the upper water column suggest preferential uptake of ^{226}Ra over Ba during formation of $SrSO_4$ skeletons by acantharians, which must contribute to barite formation in shallow waters. Deeper in the water column the $^{226}Ra_{ex}/Ba_{ex}$ ratios of suspended particles are lower than those of seawater. Since $^{228}Ra_{ex}/^{226}Ra_{ex}$ ratios demonstrate that suspended barite at these depths has been produced recently and in situ, their low $^{226}Ra_{ex}/Ba_{ex}$ ratios indicate preferential uptake of Ba over Ra in barite formed in mesopelagic water.

1. Introduction

Radium isotopes (^{228}Ra, $T_{1/2} = 5.75$ years, and ^{226}Ra, $T_{1/2} = 1602$ years) and barium (Ba) have been widely used to study ocean circulation and marine biogeochemical cycling. The global oceanic distribution of these elements and isotopes was first documented during the GEOSECS program (Broecker et al., 1967, 1976; Wolgemuth and Broecker, 1970; Bacon and Edmond, 1972; Li et al., 1973; Chan et al., 1976; Ku and Lin, 1976; Chung and Craig, 1980; Ku et al., 1980). Water column profiles of ^{226}Ra and Ba show a similar depletion in surface water and increasing deep water concentrations from the Atlantic to the Pacific Ocean. This similarity between ^{226}Ra and Ba water column profiles was attributed to the nearly identical chemical properties of the two elements (Wolgemuth and

* Corresponding author. Fax: +33 5 61 25 32 05.
E-mail address: vanbeek@notos.cst.cnes.fr (P. van Beek).
[1] Present address: University of British Columbia, Earth and Ocean Sciences Department, Vancouver, BC, Canada.
[2] Present address: Bermuda Institute of Ocean Sciences, Inc., Ferry Reach, St. Georges GE01, Bermuda.

0016-7037/$ - see front matter © 2006 Elsevier Inc. All rights reserved.
doi:10.1016/j.gca.2006.07.041

Broecker, 1970). ^{226}Ra and Ba thus show a general linear correlation over much of the water column in the Atlantic, Antarctic and Pacific Oceans, with the result that the ^{226}Ra/Ba ratio is fairly constant in the ocean (Li et al., 1973; Chan et al., 1976; Ku et al., 1980; Foster et al., 2004). Based on data from the Atlantic and Pacific Oceans, Chan et al. (1976) estimated this ratio at 4.6 nmol ^{226}Ra/mol Ba (i.e., 2.3 dpm μmol^{-1}), similar to the ratios reported in other places of the world (Li et al., 1973; Ku et al., 1980; Foster et al., 2004). In near-bottom waters, however, the correlation breaks down, with ^{226}Ra activities being higher than those predicted from the radium-barium correlation because of the input of ^{226}Ra from deep-sea sediments (Chung, 1974; Chan et al., 1976; Chung and Craig, 1980; Ku et al., 1980; Rhein and Schlitzer, 1988). This effect is particularly pronounced in the deep-northeast Pacific (Chan et al., 1976; Chung, 1976).

In contrast to ^{226}Ra, dissolved ^{228}Ra activities are highest in the upper water column and decrease rapidly through the permanent pycnocline (Kaufman et al., 1973; Li et al., 1980; Moore, 1987). The high ^{228}Ra activities in the upper water column and deep waters reflect lateral transport of ^{228}Ra that diffused from shelf sediments and release from deep-sea sediments, respectively. The low activities in intermediate waters reflect the slow vertical mixing compared to radioactive decay.

Surface depletion of Ba and ^{226}Ra results mainly from barite precipitation in the upper water column (Chow and Goldberg, 1960; Dehairs et al., 1980, 1990; Bishop, 1988; Stroobants et al., 1991). Since the world's oceans were found to be mostly undersaturated with respect to barite (Church and Wolgemuth, 1972), it was proposed that barite precipitation takes place in the upper water column within supersaturated microenvironments that result from the decay of organic matter (Chow and Goldberg, 1960; Dehairs et al., 1980; Bishop, 1988; Stroobants et al., 1991; Ganeshram et al., 2003). The correlation of particulate Ba flux and export flux of organic carbon (Dymond et al., 1992; François et al., 1995) has led to the use of barite accumulation rates in deep-sea sediments for paleoproductivity reconstructions (Schmitz, 1987; Gingele and Dahmke, 1994; Paytan et al., 1996a; Nürnberg et al., 1997).

Additionally, it has been proposed that dissolution of celestite ($SrSO_4$) skeletons made by acantharians and enriched in barium might contribute significantly to barite formation (Bernstein et al., 1987, 1992, 1998; Bernstein and Byrne, 2004). Acantharians are documented as ubiquitous and abundant marine protozoans. Their presence is especially well documented in the Sargasso Sea (Michaels, 1988; Michaels et al., 1995; Bernstein et al., 1992, 1998). Acantharians are generally concentrated in surface waters and their abundance rapidly decreases below 150 m because celestite rapidly dissolves after the death of the organism (Bishop et al., 1977, 1978; Michaels, 1988; Michaels et al., 1995; Bernstein et al., 1992). Bernstein et al. (1992) reported the presence of acantharians as deep as 400 m but specimen became very rare to non-existent in their trap located at 1500 m. These authors also described the presence of large number of cysts and minute $SrSO_4$ particles that could be related to the acantharian reproductive cycle. Because acantharians and acantharian-derived particles are enriched in barium and are also expected to incorporate radium, Bernstein et al. (1992, 1998) suggested that acantharians might play a substantial role in oceanic Ba and Ra cycling.

When barite precipitates, it acquires the ^{228}Ra/^{226}Ra ratio of the ambient seawater at the time and depth of formation (Legeleux and Reyss, 1996). Legeleux and Reyss (1996) compared the ^{228}Ra/^{226}Ra ratio of sinking particles collected with sediment traps in the tropical northeast Atlantic Ocean to that of seawater. From the sharp decrease in seawater ^{228}Ra/^{226}Ra ratio with depth, they argued that the relatively high ^{228}Ra/^{226}Ra measured in deep sediment trap material indicated that most of the particulate Ba (presumably barite) is formed in the upper 250 m of the water column. Moore and Dymond (1991) measured the ^{226}Ra/Ba ratio in sinking particles collected in the equatorial Pacific and found that particles removed ^{226}Ra and Ba from waters in the upper water column with a ratio similar to that of seawater. Also observed was a decrease in the ^{226}Ra/Ba ratios of particles with depth, which they attributed to the presence of old barite crystals (with low ^{226}Ra/Ba ratio due to ^{226}Ra decay) that were either laterally transported from continental margins or resuspended from the seafloor by deep-sea currents.

The ^{226}Ra decay in barite accumulated in deep-sea sediments has also been used to estimate Holocene sedimentation rates (Paytan et al., 1996b; van Beek and Reyss, 2001; van Beek et al., 2002, 2004). Dating of marine carbonate shells has also been attempted (Berkman and Ku, 1998; Staubwasser et al., 2004). The latter method, however, relies on knowing the initial ^{226}Ra/Ba ratio incorporated by carbonates, which can be assumed to be 4.6 nmol ^{226}Ra/mol Ba or 2.3 dpm μmol^{-1} (that is, the seawater ratio found to be fairly constant in the oceans; Chan et al., 1976). Both applications require a better understanding of the factors that control (i) the seawater Ba and ^{226}Ra distributions and (ii) the incorporation of ^{226}Ra in particulate phases such as barite or carbonates.

Analysis of radium isotopes in a particulate Ba phase such as barite can thus provide information on its origin and flux in the water column and more generally on processes such as advection, resuspension and isopycnal mixing that influence the transport of suspended particles in the ocean. In this study, we measured Ba concentrations, ^{226}Ra/Ba and ^{228}Ra/^{226}Ra ratios in seawater and in suspended and sinking particles collected at the Oceanic Flux Program (OFP) site in the western Sargasso Sea off Bermuda (31°50′N; 64°10′W; 4500 m water depth) to track barite formation and transport in the water column. To our knowledge, this work reports the first ^{226}Ra and ^{228}Ra activities measured in suspended particles. This allowed us to combine seawater data with data from both the

sinking and suspended particle pools. Additionally, because previous studies reported abundant acantharian populations in the Sargasso Sea, which might influence the Ba and Ra distributions, Sr contents were analyzed in suspended particles to track the presence of acantharians.

2. Materials and methods

2.1. Sample collection

The Oceanic Flux Program (OFP) sediment trap time-series mooring (Conte et al., 2001) is located in the northern Sargasso Sea in a transitional region between relatively eutrophic waters to the north and oligotrophic subtropical waters to the south. In addition to the OFP sediment trap time-series, the area is the site of the Bermuda-Atlantic Times Series (BATS, Steinberg et al., 2001) and the Bermuda testbed Mooring (BTM, Dickey et al., 2001).

Seawater samples were collected at the OFP site in May 2002 (from fourth to eighth) using a CTD equipped with 12-liter Niskin bottles. Sixty milliliter samples were collected for dissolved Ba measurements. For Ra isotopes, 50–60 L of seawater was passed through a cartridge filled with MnO_2-coated fibers that retain radium isotopes (Moore and Reid, 1973; Moore et al., 1985). The fibers were then ashed (1 day at 820 °C) and transferred into counting vials for gamma counting.

Suspended particles were collected using McLane large volume in situ pumps (WTS, McLane Labs, Falmouth Ma, USA). Up to 2300 L was filtered through 142-mm diameter Versapor filters (acrylic copolymer on a nylon substrate; Pall Corporation), with a pore size of 0.8 μm.

Sinking particles were collected using Parflux Mark VII sediment traps (McLane Labs, Falmouth MA, USA). Details of OFP sample collection and processing are given in Conte et al. (2001). Sediment trap samples were analyzed from both the 1500 and 3200 m depth traps. Analyses were conducted on archived dried material collected in 1988–1989 and 1999–2000. The integrated sampling period ranges between 58–76 days in 1988–1989 and 14–15 days in 1999–2000 (Table 3).

2.2. Analytical methods

2.2.1. Seawater

Seawater was analyzed for barium by isotope dilution using a ^{135}Ba spike (precision: ±2% estimated from replicate analyses), using the Inductively Coupled Plasma Mass Spectrometry (ICP-MS) facility at Woods Hole Oceanographic Institution (Element, Finnigan). Radium isotopes adsorbed on MnO_2 ash were counted at the underground laboratory of Modane (Laboratoire Souterrain de Modane, French Alps). High-efficiency, low-background, well-type germanium detectors (215, 430 and 950 cm^3) were used (Reyss et al., 1995). These detectors are shielded from cosmic radiation by 1700 m of rocks; a very low background is thus achieved, allowing the measurement of very low activities. ^{226}Ra activities were determined using the ^{214}Pb (295 and 352 keV) and ^{214}Bi (609 keV) peaks. ^{228}Ra activities were determined using the 338, 911 and 969 keV peaks of ^{228}Ac. Counting time for each sample ranges from 2 to 5 days. Uncertainties reported for ^{226}Ra and ^{228}Ra activities are errors due to counting statistics.

2.2.2. Suspended particles

Results reported here for particles are based on bulk analyses. Ra isotopes were first measured on intact filters by gamma counting using the same method used for the MnO_2 ashed samples. The Versapor filters were subsequently dissolved in a Teflon beaker with a mixture of HNO_3 (ultrapure acid), HF (ultrapure acid), and $HClO_4$ (pure acid) placed on a hot plate. Barium and strontium concentrations were measured at LEGOS by ICP-MS using a Elan 6000 Perkin-Elmer (reproducibility of the method estimated at ±4%) using external standards. Na and Ca were analyzed by atomic spectrophotometry at OMP (Observatoire Midi Pyrénées), Toulouse. ^{232}Th was measured by ICP/MS (VG PlasmaQuad II) at the Scottish Universities Research and Reactor Centre, East Kilbride, also using external standards (reproducibility of the method estimated at ±4%).

Particulate Ba and Ra are mainly associated with barite in the water column (Dehairs et al., 1980, 1990). We calculated excess Ba concentration (Ba_{ex}) and excess Ra activities ($^{226}Ra_{ex}$ and $^{228}Ra_{ex}$) in suspended particles that refer to the Ba and Ra associated with barite. Ba and Ra concentrations were corrected for lithogenic fraction using the following equations:

$$Ba_{ex} = Ba_{measured} - (^{232}Th_{measured} \times [Ba/^{232}Th]_{upper\ crust}), \quad (1)$$

$$^{226}Ra_{ex} = {}^{226}Ra_{measured} - (^{232}Th_{measured} \times [^{238}U/^{232}Th]_{upper\ crust}), \quad (2)$$

$$^{228}Ra_{ex} = {}^{228}Ra_{measured} - (^{232}Th_{measured}), \quad (3)$$

where $Ba_{measured}$, $^{226}Ra_{measured}$ and $^{228}Ra_{measured}$ refer to the total concentrations or activities. We used the value of 51.4 (ppm/ppm) for the $[Ba/^{232}Th]_{upper\ crust}$ ratio, which is the mean ratio for the upper crust reported by Taylor and McLennan (1985); ^{226}Ra and ^{228}Ra activities were corrected for the activities in radioactive equilibrium with lithogenic ^{238}U and ^{232}Th, respectively. The ^{232}Th activities measured were assumed to be entirely lithogenic. The lithogenic ^{238}U activities were estimated from the ^{232}Th activities, using the upper continental crust $^{238}U/^{232}Th$ ratio of 0.8 (dpm/dpm; Taylor and McLennan, 1985; Anderson et al., 1990). While oceanic particles may often contain an authigenic U fraction, this is assumed to be too recent to be associated with significant ^{226}Ra ingrowth. Errors on the excess concentrations were obtained by propagating the errors of each elemental concentrations (Ba, ^{226}Ra, ^{228}Ra as well as ^{232}Th). It should be stressed here that errors associated with the estimate and the use of mean lithogenic ratios to calculate the lithogenic Ba and Ra

fractions may introduce errors in the calculated excess Ba and Ra concentrations.

As $SrSO_4$ is the major structural component of acantharians, we measured Sr concentrations in particles to track the presence of acantharians. Sr in particles may also be associated with carbonates. Following Bishop et al. (1977), we estimated non-carbonate Sr concentrations that will be related to acantharians:

$$\text{non-carbonate Sr} = \text{Sr}_{\text{measured}} - (\text{Sr}_{\text{seawater}} + \text{Sr}_{\text{carbonate}}). \quad (4)$$

First, we corrected the Sr concentrations determined from filters collected with in situ pumps for the sea-salt contribution by analyzing the Na content and considering a Sr/Na ratio in seawater of 0.00019 (mol/mol). The Sr content of the carbonate fraction was calculated assuming that carbonates contained 0.17 mol% Sr (Bishop et al., 1977). Carbonate content was estimated from the Ca concentration corrected for (i) the sea-salt contribution (using a Ca/Na ratio of 0.0219 mol/mol in seawater) and (ii) the lithogenic Ca phase using a crustal Ca/Th ratio (ppm/ppm) of 2804 (Taylor and McLennan, 1985). The lithogenic Sr contribution can be neglected. Uncertainty on particulate Sr concentrations is estimated at 10% due to the different corrections (propagation of errors). Again, the use of a mean crustal Ca/Th ratio to calculate the lithogenic Ca may introduce errors in the calculated Ca associated with carbonates. Correction for the Sr associated with sea salt is ca. 35% for most samples but is higher for samples above 200 m (ca. 50%) and reaches 83% for the 20 m pump sample. Sr associated with carbonates represents 15–30% of the total Sr, but is only 3% for sample collected at 20 m.

2.2.3. Sinking particles

Sediment trap samples were first analyzed for Ra isotopes by gamma counting at Modane. Barium and ^{232}Th were then measured by instrumental neutron activation (at Laboratoire des Sciences du Climat et de l'Environnement, LSCE, Gif-sur-Yvette, France) for samples collected in 1988–1989 and ICP/MS (Elan 6000 Perkin-Elmer; OMP, Toulouse) for samples collected in 1999–2000. For neutron activation analysis, samples were placed 5 min under a neutron flux of 1.1×10^{14} neutrons cm^{-2} s^{-1} in the Osiris nuclear reactor at Laboratoire Pierre Süe (Saclay, France). Samples were then measured for their radioactivity using the germanium detectors located at LSCE, Gif-sur-Yvette, France (precision: ±5% estimated from replicate analyses of standards). For ICP/MS measurements, samples were digested in a microwave using a mixture of HF and HNO_3 prior to analysis (precision: ±3% estimated from replicate analyses of standards).

Excess Ba, ^{226}Ra and ^{228}Ra were calculated as explained in the suspended particles section. $^{228}Ra_{ex}$ activities of sinking particles were also corrected for radioactive decay since the time of sampling (denoted $^{228}Ra_{ex}°$ in Table 3). In contrast, ^{228}Ra activities of suspended particles and seawater samples were not decay-corrected because gamma counting of the samples was performed within the 5 months following sample collection.

3. Results

3.1. Hydrography

The vertical structure and circulation of water masses in the region has been previously reviewed by Talley (1996), Joyce and Robbins (1996) and references therein. A CTD profile collected on the OFP cruise (early May 2002) and discrete nutrient data collected on an earlier BATS cruise (mid-April 2002) provided information on vertical structure of water masses that was pertinent to the samples collected (Fig. 1). Below a 30-m surface mixed layer, variable salinity indicated a complex water mass structure within and below the seasonal thermocline, including a distinctive lense of fresher water lying between 160 and 180 m. Subtropical Mode Water ("18 °C water"), which outcrops in the northern Sargasso Sea just south of the Gulf Stream, was found between 275 and 400 m. The depth of the O_2 minimum was 890 m, just above the maxima in AOU, NO_3^- and PO_4^{3-}. An influence of westward spreading Mediterranean water is suggested by positive excursions in salinity and negative excursions in O_2 and PO_4^{3-} at depths between 980–1200 and 1300–1470 m. The core of the southward flowing Labrador Sea Water (LSW), a high oxygen and low salinity water mass of σ_θ 27.78, was centered at 1650 m, above the North Atlantic Deep Water. Antarctic Bottom Water (AABW), identified by a potential $T < 1.90$ °C and high nutrients, was present below 3800 m.

3.2. Elemental concentrations and ratios

3.2.1. Barium and radium in seawater

Dissolved Ba, ^{226}Ra and ^{228}Ra profiles (Fig. 2; Table 1) are similar to those reported earlier for the Atlantic Ocean (Broecker et al., 1967, 1976; Wolgemuth and Broecker, 1970; Kaufman et al., 1973; Chan et al., 1976, 1977; Moore et al., 1985; Kim et al., 2003). Barium concentrations and ^{226}Ra activities in seawater increase with depth, reflecting uptake during particle formation in shallow waters and subsequent release to the deep water from settling particles. Ba and ^{226}Ra contents are relatively constant in the upper 400 m (ca. 44.4 nmol kg^{-1} Ba; ca. 8.6 dpm/100 kg ^{226}Ra) and increase with increasing water depth. ^{226}Ra activities increase in two steps to a maximum of 17.5 dpm/100 kg near the seafloor. The steep increase in Ba concentrations and ^{226}Ra activities below 3700 m can be explained by the presence of Antarctic Bottom Water which are enriched in Ba and ^{226}Ra (Broecker et al., 1976; Li et al., 1973; Jacquet et al., 2004) and by the input of Ba and ^{226}Ra from the sediments. The ^{228}Ra activity profile at the OFP site displays a strong vertical gradient from surface to intermediate waters. ^{228}Ra activities increase again close to the bottom due to diffusion from deep-sea sediments. Calculation

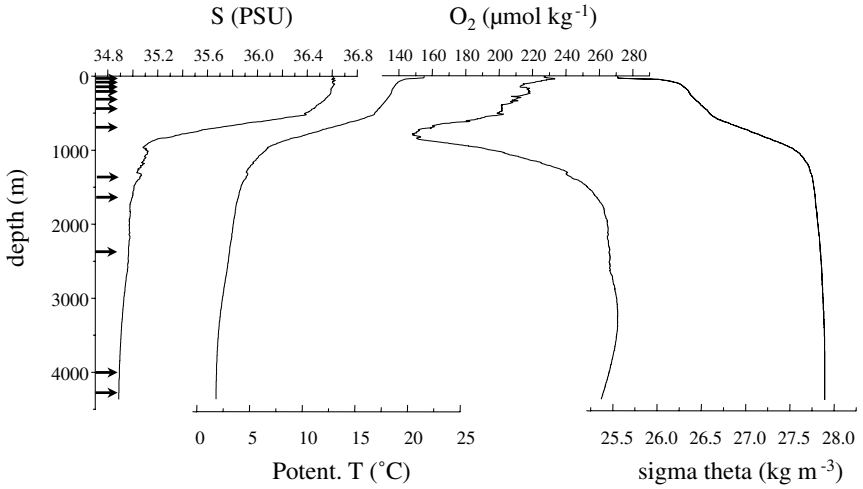

Fig. 1. Hydrography at the OFP site. Profiles of salinity, potential temperature, oxygen and density are reported. Arrows indicate the depths of sample collection (suspended particles and seawater).

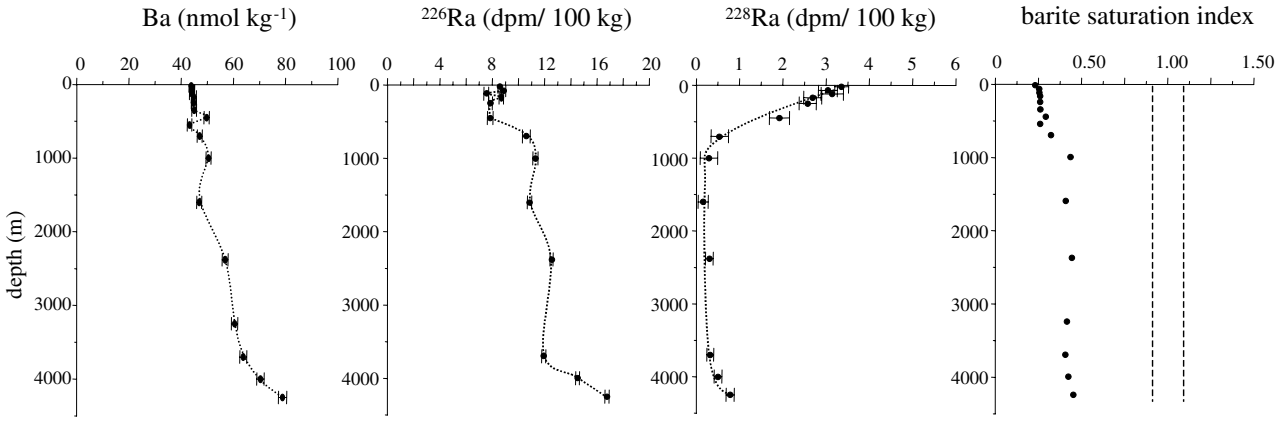

Fig. 2. Dissolved Ba, ^{226}Ra and ^{228}Ra profiles. The barite saturation index profile is also reported. Calculations were made by C. Monnin, LMTG, Toulouse, following Monnin et al. (1999). Pure barite was considered in the calculations. Equilibrium is reached for a saturation index of 1.0 (0.9–1.1). Undersaturation is indicated by a saturation index smaller than 1.0.

Table 1
Results of measurements conducted in seawater

Depth (m)	Ba (nmol kg^{-1}) (±2%)	^{226}Ra (dpm/100 kg)	^{228}Ra (dpm/100 kg)	$^{228}Ra/^{226}Ra$	$^{226}Ra/Ba$ (dpm μmol^{-1})
20	43.90	8.71 ± 0.12	3.42 ± 0.16	0.39 ± 0.02	1.98 ± 0.05
70	44.32	9.21 ± 0.18	3.16 ± 0.23	0.34 ± 0.03	2.08 ± 0.06
120	44.09	7.82 ± 0.19	3.26 ± 0.27	0.42 ± 0.04	1.77 ± 0.06
170	44.84	8.96 ± 0.17	2.77 ± 0.22	0.31 ± 0.02	2.00 ± 0.06
250	44.80	8.16 ± 0.14	2.67 ± 0.20	0.33 ± 0.03	1.82 ± 0.05
350	45.00				
450	49.80	8.20 ± 0.22	2.01 ± 0.24	0.25 ± 0.03	1.65 ± 0.06
550	43.21				
700	47.12	10.98 ± 0.31	0.56 ± 0.21	0.05 ± 0.02	2.33 ± 0.08
1000	50.52	11.67 ± 0.21	0.30 ± 0.21	0.03 ± 0.02	2.31 ± 0.06
1600	46.92	11.21 ± 0.17	0.16 ± 0.12	0.01 ± 0.01	2.39 ± 0.06
2380	56.87	12.94 ± 0.12	0.31 ± 0.09	0.02 ± 0.01	2.28 ± 0.05
3250	60.48				
3700	63.81	12.49 ± 0.16	0.33 ± 0.08	0.03 ± 0.01	1.96 ± 0.05
4000	70.37	15.20 ± 0.16	0.52 ± 0.09	0.03 ± 0.01	2.16 ± 0.05
4250	78.82	17.50 ± 0.17	0.81 ± 0.09	0.05 ± 0.01	2.22 ± 0.05

of the barite saturation index indicates that waters at the OFP site are undersaturated with respect to barite (Fig. 2). This pattern agrees with Monnin et al. (1999) who concluded that the whole Atlantic Ocean was undersaturated with respect to barite. The barite saturation index profile suggests that once barite is formed in supersaturated microenvironments at the OFP site, barite is subject to dissolution.

3.2.2. Barium and radium in suspended particles

3.2.2.1. Barium. Particulate barium concentrations are higher in the upper 1500 m and especially in the upper 500 m (Fig. 3). They are low at 20 m but peak at 70 m (0.24 nmol kg^{-1}) and 300 m (0.18 nmol kg^{-1}). These concentrations are in the same range as the values reported by Bishop (1988) in the Sargasso Sea. They are two orders of magnitude lower than the dissolved Ba concentrations. Barite is generally considered the main carrier (Dehairs et al., 1980, 1990, 1991; Bishop, 1988), with a smaller contribution from lithogenic material. To correct for the latter, excess Ba concentrations (Ba_{ex}) were calculated by subtracting lithogenic Ba estimated from particulate ^{232}Th concentrations. The lithogenic fraction is relatively small and constant throughout the water column but increases sharply below ca. 4000 m, reflecting the presence of a bottom nepheloid layer (Fig. 3; Table 2). Sherrell and Boyle

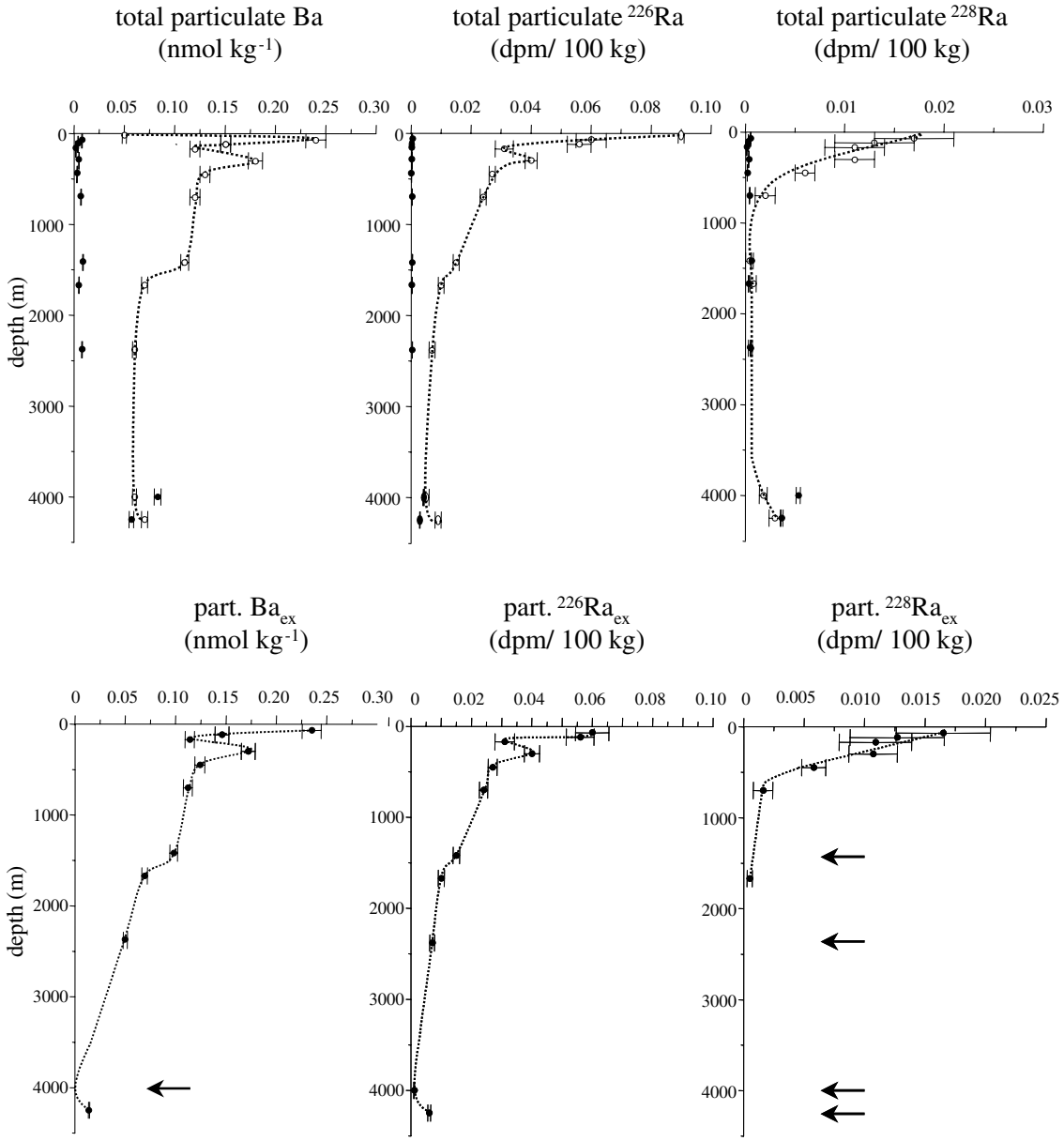

Fig. 3. The upper panels show Ba, ^{226}Ra and ^{228}Ra profiles in suspended particles while the lower panels show excess Ba, ^{226}Ra and ^{228}Ra profiles in suspended particles (that is, total contents corrected for the lithogenic fraction). In the upper panel, open circles represent total Ba concentrations, total ^{226}Ra and ^{228}Ra activities, respectively, whereas solid circles represent the concentrations associated with the lithogenic fraction. Arrows on the lower panel indicate the depths where no significant Ba_{ex} or $^{228}Ra_{ex}$ activities were measured in the suspended particles.

Table 2
Results of measurements conducted in suspended particles (in situ pumps)

Depth (m)	^{226}Ra (dpm/100 kg)	^{228}Ra (dpm/100 kg)	^{232}Th (dpm/100 kg) (±4%)	Lithogenic ^{238}U[a] (dpm/100 kg) (±4%)	$^{226}Ra_{ex}$ (dpm/100 kg)	$^{228}Ra_{ex}$ (dpm/100 kg)	$^{228}Ra_{ex}/^{226}Ra_{ex}$	Ba (nmol kg^{-1}) (±4%)	Lithogenic Ba[b] (nmol kg^{-1}) (±4%)	Ba_{ex} (nmol kg^{-1}) (±4%)	$^{226}Ra_{ex}/Ba_{ex}$ (dpm µmol^{-1})	Sr[c] (nmol kg^{-1}) (±10%)	Non-carbonate Sr[d] (nmol kg^{-1}) (±10%)
20	0.090 ± 0.001	0.0710 ± 0.0160	n.m.	—	—	—	—	0.048	—	—	—	0.302	0.248
70	0.060 ± 0.005	0.0170 ± 0.0040	0.00053	0.00042	0.060 ± 0.0055	0.0165 ± 0.0039	0.276 ± 0.071	0.243	0.008	0.235	2.54 ± 0.26	0.508	0.086
120	0.056 ± 0.004	0.0130 ± 0.0040	0.00029	0.00023	0.056 ± 0.0046	0.0127 ± 0.0039	0.228 ± 0.073	0.150	0.004	0.146	3.83 ± 0.35	0.421	0.257
170	0.031 ± 0.003	0.0110 ± 0.0030	0.00015	0.00012	0.031 ± 0.0032	0.0109 ± 0.003	0.351 ± 0.104	0.116	0.002	0.114	2.71 ± 0.30	0.183	0.122
300	0.040 ± 0.002	0.0110 ± 0.0020	0.00035	0.00028	0.040 ± 0.0025	0.0107 ± 0.0020	0.268 ± 0.053	0.177	0.005	0.172	2.31 ± 0.17	0.211	0.128
450	0.027 ± 0.001	0.0060 ± 0.0010	0.00021	0.00017	0.027 ± 0.0015	0.0058 ± 0.0010	0.216 ± 0.039	0.127	0.003	0.124	2.17 ± 0.15	0.164	0.101
700	0.024 ± 0.001	0.0020 ± 0.0010	0.00043	0.00034	0.024 ± 0.0014	0.0016 ± 0.0008	0.066 ± 0.034	0.119	0.007	0.112	2.10 ± 0.15	0.155	0.096
1420	0.015 ± 0.001	0.0004 ± 0.0004	0.00058	0.00046	0.015 ± 0.0011	0	0	0.107	0.009	0.098	1.49 ± 0.13	0.152	0.088
1670	0.010 ± 0.001	0.0008 ± 0.0003	0.00033	0.00026	0.010 ± 0.0010	0.0005 ± 0.0002	0.048 ± 0.019	0.074	0.005	0.069	1.41 ± 0.16	0.109	0.069
2380	0.007 ± 0.001	0.0005 ± 0.0002	0.00053	0.00042	0.007 ± 0.0008	0	0	0.059	0.008	0.050	1.33 ± 0.16	0.100	0.058
4000	0.005 ± 0.001	0.0018 ± 0.0004	0.00532	0.00425	0.001 ± 0.0001	0	0	0.057	0.083	0	0	0.102	0.074
4250	0.009 ± 0.001	0.0030 ± 0.0006	0.00365	0.00292	0.006 ± 0.0005	0	0	0.070	0.057	0.014	4.78 ± 0.41	0.098	0.048

n.m., not measured.
[a] Derived from the ^{232}Th activities considering a lithogenic U/Th ratio of 0.8 (dpm/dpm) after Taylor and McLennan (1985).
[b] Derived from the ^{232}Th activities using $Ba/^{232}Th$ of the upper crust after Taylor and McLennan (1985).
[c] Sr content corrected for Sr associated with sea salt.
[d] Sr content further corrected for Sr associated with $CaCO_3$.

(1992) reported a similar increase in particulate Al and Fe concentrations towards the bottom in the water column near Bermuda. Using their Al data and a Ba/Al ratio of 0.0075, we obtain lithogenic Ba concentrations which are in good agreement with our estimates. The lithogenic correction is small in the upper 1500 m and Ba_{ex} concentrations remain high (Fig. 3). In contrast, the Ba content of suspended particles collected in deep waters is dominated by lithogenic Ba, and no Ba_{ex} could be found in the upper nepheloid layer, indicating a substantial decrease in suspended barite concentration with depth. Note that the lithogenic Ba deduced from ^{232}Th concentrations is higher than the Ba content measured in sample collected at 4000 m. Uncertainty associated with the crustal Ba/Th ratio used to calculate the lithogenic Ba may explain such pattern.

3.2.2.2. Radium isotopes. ^{226}Ra activities in suspended particles are highest in surface waters (0.09 dpm/100 kg, i.e., two orders of magnitude lower than the ^{226}Ra activity in seawater) and decrease with depth, with a secondary peak at 300 m (Fig. 3). The excess ^{226}Ra profile is similar to that of excess Ba (Fig. 3). Suspended $^{226}Ra_{ex}$ activities are highest in the upper 500 m, where the lowest dissolved ^{226}Ra activities are found (Fig. 2), and decrease with depth before increasing slightly towards the seafloor. Particulate ^{228}Ra activities are also highest towards the surface and decrease rapidly to very low values in mid water. Very little or no excess ^{228}Ra activity remains in suspended particles below 1000 m. For the sample collected at 4000 m, note that the ^{232}Th activity is higher than that of ^{228}Ra.

3.2.3. $^{228}Ra/^{226}Ra$ and $^{226}Ra/Ba$ ratios in seawater and suspended particles

3.2.3.1. $^{228}Ra/^{226}Ra$ ratios. The dissolved $^{228}Ra/^{226}Ra$ seawater profile shows a strong vertical gradient in the upper water column as it was observed for the ^{228}Ra activities (Fig. 4). Our data agree with those of Kim et al. (2003) who reported $^{228}Ra/^{226}Ra$ ratios from the upper 600 m in the same area. $^{228}Ra_{ex}/^{226}Ra_{ex}$ activity ratios in suspended particles (Fig. 4 and Table 2) display a profile similar to that of $^{228}Ra_{ex}$ activities. $^{228}Ra_{ex}/^{226}Ra_{ex}$ ratios found in suspended particles match the seawater ratios down to 2000 m depth.

3.2.3.2. $^{226}Ra/Ba$ ratios. The dissolved $^{226}Ra/Ba$ ratios below 500 m are close to 2.3 dpm µmol^{-1} (that is, the value reported by Chan et al., 1976), which can be considered as a reference value, but we find significantly lower values in the upper 500 m of the water column, above the main thermocline (Fig. 5). $^{226}Ra_{ex}/Ba_{ex}$ ratios in suspended particles collected in the upper 170 m are higher than 2.3 dpm µmol^{-1}, reaching a maximum (3.8 dpm µmol^{-1}) at 120 m depth (Fig. 5). Such values are higher than the maximum value reported by Moore and Dymond (1991) when analyzing sediment trap material from the Pacific Ocean. Below 120 m, $^{226}Ra_{ex}/Ba_{ex}$ ratios exhibit a

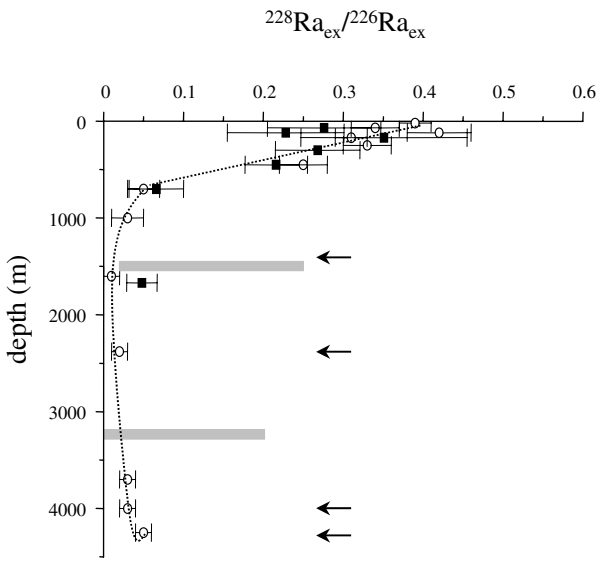

Fig. 4. $^{228}Ra_{ex}/^{226}Ra_{ex}$ ratios in suspended particles (solid squares) reported together with the ratios found in seawater (open circles). Arrows indicate the depths where no significant $^{228}Ra_{ex}$ were measured in the suspended particles. As a comparison, the shaded bars represents the range of values found in sinking particles (at 1500 and 3200 m, respectively).

constant decrease with increasing depth. From 300 to 700 m, $^{226}Ra_{ex}/Ba_{ex}$ ratios are close to the value of 2.3 dpm μmol^{-1}. Below 1000 m, $^{226}Ra_{ex}/Ba_{ex}$ ratios are lower, with values as low as 1.33 dpm μmol^{-1} at 2380 m. $^{226}Ra_{ex}/Ba_{ex}$ ratios in the bottom nepheloid layer may be questionable because $^{226}Ra_{ex}$ and Ba_{ex} concentrations at these depths are small compared to their lithogenic fraction which make them very sensitive to the uncertainties in the lithogenic correction.

As a comparison, Sr contents were also analyzed in suspended particles. Sr contents are also high in the upper 150 m (Fig. 5). Sr values (total Sr corrected for sea salt as well as non-carbonate Sr) are similar to values reported by Bishop et al. (1977, 1978) who analyzed suspended particles also collected using in situ pumps in the Atlantic Ocean. Maximum non-carbonate Sr concentrations are found at 120 m. Below this depth, non-carbonate Sr concentrations decrease with increasing water depth down to ca. 1500 m. Deeper in the water column, Sr contents display constant values.

3.2.4. Ratios in sinking particles (sediment traps)

3.2.4.1. $^{228}Ra_{ex}/^{226}Ra_{ex}$ ratio. The range of $^{228}Ra_{ex}/^{226}Ra_{ex}$ ratios found in sinking particles collected during the two different periods is very similar (Fig. 6, Table 3). In most cases, the ratios range between 0.1 and 0.2, with significant variability. Note that for several samples from the deeper sediment trap, no significant excess ^{228}Ra activities could be found. In most cases the ratio found in the deep sediment trap at 3200 m is lower than the ratio found at 1500 m.

3.2.4.2. $^{226}Ra_{ex}/Ba_{ex}$ ratio. $^{226}Ra_{ex}/Ba_{ex}$ ratios also display significant variability with time and water depth (0.53–4.09 dpm μmol^{-1}, Fig. 7). In most cases, the $^{226}Ra_{ex}/Ba_{ex}$ ratio found at 3200 m is lower than the ratio found at 1500 m, with, however, two samples showing the opposite trend (i.e., February–April 1989 and June 2000). Two samples collected at 1500 m in 1988 (i.e., March–May and July–September) display $^{226}Ra_{ex}/Ba_{ex}$ ratios much higher than the seawater ratio (>3.5 dpm μmol^{-1}). Sediment trap material from the Pacific Ocean analyzed by Moore and Dymond (1991) did not exhibit such high values. $^{226}Ra_{ex}/Ba_{ex}$ ratios found in samples collected in 1999–2000 were all <2.1 dpm μmol^{-1}, with most of the samples displaying ratios lower than the seawater ratios reported in this study (<1.5 dpm μmol^{-1}).

4. Discussion

4.1. $^{228}Ra_{ex}/^{226}Ra_{ex}$ ratios

Previous studies have suggested that barite precipitation takes place mainly in the upper 500 m of the water column

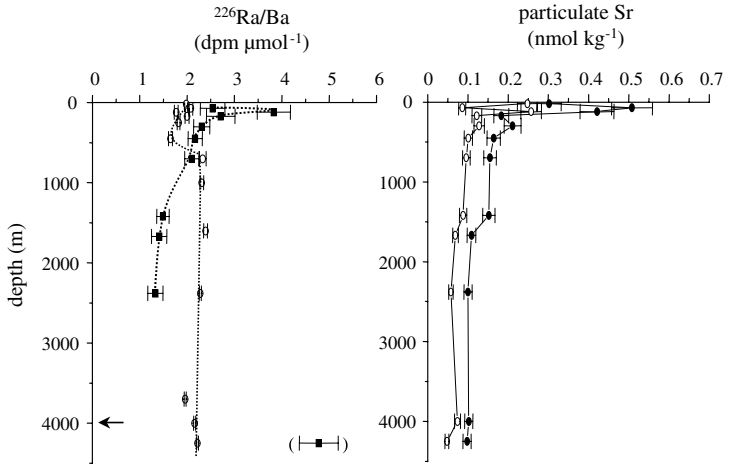

Fig. 5. (Left panel) $^{226}Ra/Ba$ ratios in seawater (open circles) reported together with $^{226}Ra_{ex}/Ba_{ex}$ ratios in suspended particles (closed squares). (Right panel) Sr content measured in suspended particles. Solid circles represent the total Sr content (corrected for the Sr associated with sea salt) while open circles consist in the non-carbonate Sr.

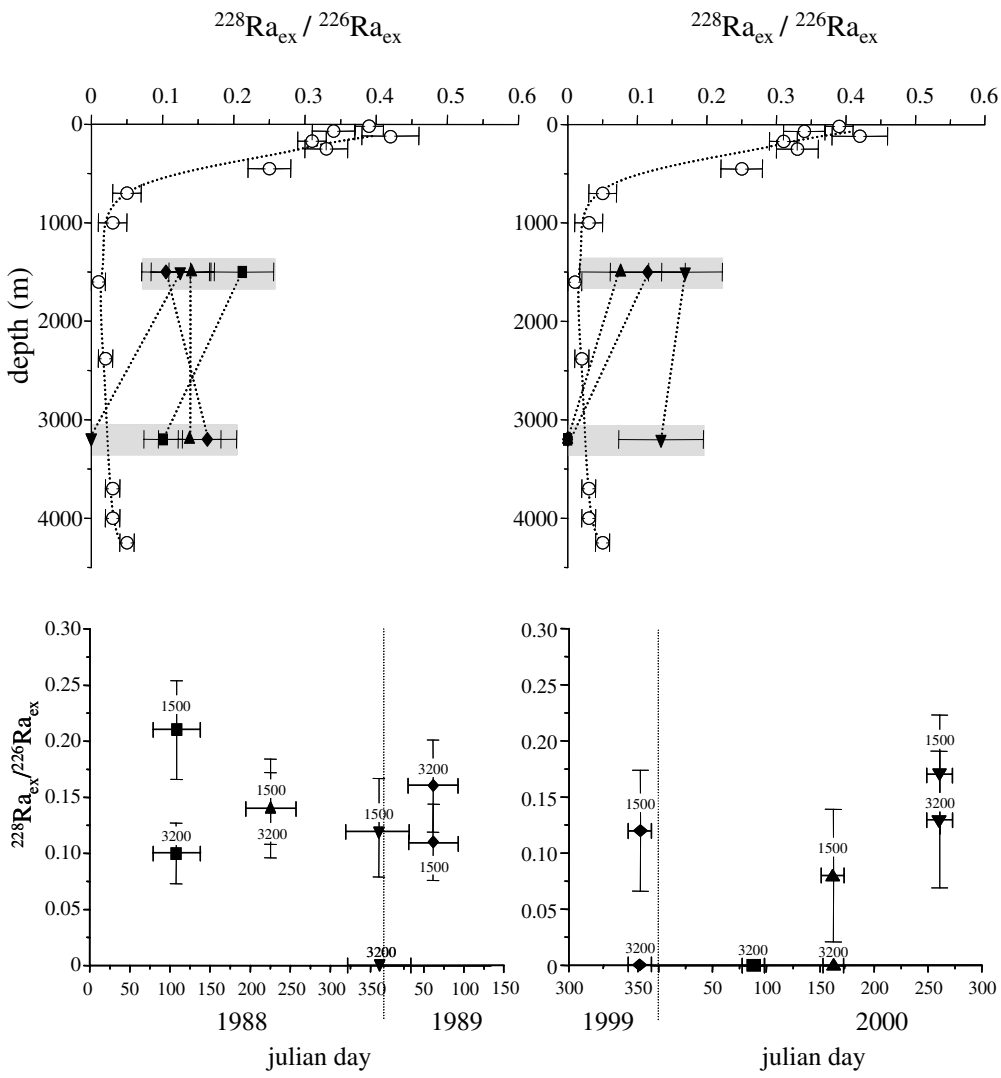

Fig. 6. $^{228}Ra_{ex}/^{226}Ra_{ex}$ ratios in sinking particles collected with sediment traps reported versus water depth (upper panels) and versus time (lower panels). Solid symbols represent the ratios found in sinking particles whereas open circles represent the seawater ratios obtained during the 2002 cruise. Results obtained on samples collected in 1988–1989 are reported on the left panel, while those from samples collected in 1999–2000 are reported on the right panel. Width of the plots on the lower panels indicates sampling duration. (Left panels) Solid squares: 19 March–17 May 1988 (58 days collection); up triangles: 13 July–13 September 1988 (61 days collection); down triangles: 15 November 1988–1 February 1989 (76 days collection); diamonds: 1 February–4 April 1989 (61 days collection). (Right panels) Diamonds: 10 December 1999–25 December 1999 (15 days collection); solid squares: 23 March 2000–5 April 2000 (14 days collection); up triangles: 5 June 2000–20 June 2000 (15 days collection); down triangles: 5 September 2000–20 September 2000 (15 days collection).

(Chow and Goldberg, 1960; Dehairs et al., 1980, 1990, 1991, 1992; Bishop, 1988; Legeleux and Reyss, 1996), which could account for the higher particulate excess Ba and ^{226}Ra concentrations found in the upper 500 m at the OFP site. Suspended barite found deeper in the water column could have been produced in situ (that is, at the depth of sample collection) or could have been released from aggregates settling from shallower depth. When studying suspended particles in the Sargasso Sea, Bishop (1988) concluded that barite crystals formed in the >53 μm particle size fractions in near-surface waters and were released into the 1–53 μm fraction at depths below the euphotic zone (at 200–300 m). Such release could occur also deeper in the water column. The decreasing trend in Ba_{ex} and $^{226}Ra_{ex}$ particulate concentrations with depth (Fig. 3) could thus reflect a decrease in supply of fine barite crystals by breakdown of settling particles which is expected to be more intensive in the upper 500 m. Once released from the supersaturated microenvironments in which they presumably formed, barite crystals would be subject to dissolution in undersaturated waters (Fig. 2; Church and Wolgemuth, 1972; Monnin et al., 1999; Rushdi et al., 2000; Monnin and Cividini, 2006). Thus, the decrease in particulate Ba_{ex} and $^{226}Ra_{ex}$ with depth could also be partly driven by gradual dissolution during settling. In addition, barite may also precipitate below 500 m, which would require the presence of supersaturated microenvironments at these depths. The decreasing trend of Ba_{ex} profile could thus reflect a decrease in the rate at which barite is produced in situ. With its strong gradient in the upper water column,

Table 3
Results of measurements conducted in sinking particles (sediment traps)

Sample	Depth (m)	Sampling duration (d)	Total flux (mg m^{-2} d^{-1})	^{226}Ra (dpm g^{-1})	^{228}Ra (dpm g^{-1})	^{232}Th[a] (dpm g^{-1}) (±5%)	^{232}Th[b] (dpm g^{-1}) (±3%)	^{238}U[c] (dpm g^{-1})	$^{226}Ra_{ex}$ (dpm g^{-1})	$^{228}Ra_{ex}$ (dpm g^{-1})	$^{228}Ra°_{ex}$ (dpm g^{-1})	$^{228}Ra°_{ex}$/ $^{226}Ra_{ex}$	Ba_{ex} (ppm) (±3%)	$^{226}Ra_{ex}$/ Baex (dpm μmol^{-1})	Ba_{ex} flux (μmol m^{-2} d^{-1})
March–May 1988	1500	58	59.8	11.46 ± 0.22	0.79 ± 0.11	0.33	—	0.26	11.20 ± 0.60	0.46 ± 0.07	2.37 ± 0.35	0.21 ± 0.044	433	3.55 ± 0.22	0.19
March–May 1988	3200	58	49.3	8.56 ± 0.17	0.67 ± 0.12	0.51	—	0.41	8.15 ± 0.44	0.16 ± 0.03	0.82 ± 0.15	0.10 ± 0.027	504	2.22 ± 0.14	0.18
July–September 1988	1500	61	31.7	9.30 ± 0.19	0.85 ± 0.13	0.60	—	0.48	8.82 ± 0.48	0.25 ± 0.04	1.24 ± 0.20	0.14 ± 0.032	296	4.09 ± 0.25	0.07
July–September 1988	3200	61	36.4	7.96 ± 0.23	0.77 ± 0.17	0.56	—	0.45	7.51 ± 0.43	0.21 ± 0.05	1.04 ± 0.24	0.14 ± 0.044	799	1.29 ± 0.08	0.21
November 1988–January 1989	1500	76	29.2	10.14 ± 0.23	0.91 ± 0.21	n.m.	0.65	0.52	9.62 ± 0.36	0.26 ± 0.06	1.20 ± 0.28	0.12 ± 0.041	872	1.52 ± 0.07	0.19
November 1988–January 1989	3200	76	37.8	7.66 ± 0.22	0.69 ± 0.20	0.73	—	0.58	7.08 ± 0.41	0	0	0	798	1.22 ± 0.08	0.22
January–April 1989	1500	61	50.9	9.24 ± 0.20	0.77 ± 0.17	0.57	—	0.46	8.78 ± 0.48	0.20 ± 0.05	0.92 ± 0.21	0.11 ± 0.034	716	1.69 ± 0.10	0.27
January–April 1989	3200	61	58.4	7.58 ± 0.15	0.87 ± 0.15	0.62	—	0.50	7.08 ± 0.38	0.25 ± 0.04	1.16 ± 0.21	0.16 ± 0.041	406	2.40 ± 0.15	0.17
December 1999	1500	15	29.7	9.30 ± 0.51	1.28 ± 0.42	—	0.55	0.44	8.86 ± 0.55	0.73 ± 0.24	1.02 ± 0.34	0.12 ± 0.054	908	1.34 ± 0.09	0.20
December 1999	3200	15	24.8	6.76 ± 0.54	0.53 ± 0.25	—	0.81	0.65	6.11 ± 0.52	0	0	0	825	1.02 ± 0.09	0.15
March 2000	1500	14	57.9	7.21 ± 0.41	2.53 ± 0.38	—	n.m.	n.m.	—	—	—	—	—	—	—
March 2000	3200	14	61.2	3.04 ± 0.09	0.57 ± 0.07	—	0.56	0.45	2.59 ± 0.11	0	0	0	666	0.53 ± 0.03	0.30
June 2000	1500	15	28.7	8.13 ± 0.73	1.04 ± 0.57	—	0.58	0.47	7.66 ± 0.73	0.46 ± 0.25	0.58 ± 0.32	0.08 ± 0.059	1042	1.01 ± 0.10	0.22
June 2000	3200	15	19.9	10.10 ± 0.87	0.39 ± 0.28	—	0.64	0.51	9.59 ± 0.87	0	0	0	654	2.01 ± 0.19	0.09
September 2000	1500	15	34.6	6.30 ± 0.29	1.38 ± 0.30	—	0.62	0.50	5.80 ± 0.32	0.76 ± 0.17	0.98 ± 0.22	0.17 ± 0.053	723	1.10 ± 0.07	0.18
September 2000	3200	15	35.1	5.95 ± 0.49	1.23 ± 0.39	—	0.64	0.51	5.44 ± 0.48	0.59 ± 0.19	0.73 ± 0.24	0.13 ± 0.061	719	1.04 ± 0.10	0.18

n.m., not measured.
[a] Neutron activation.
[b] ICP/MS.
[c] Lithogenic ^{238}U determined from ^{232}Th; ±3% for ICP/MS and ±5% for neutron activation.

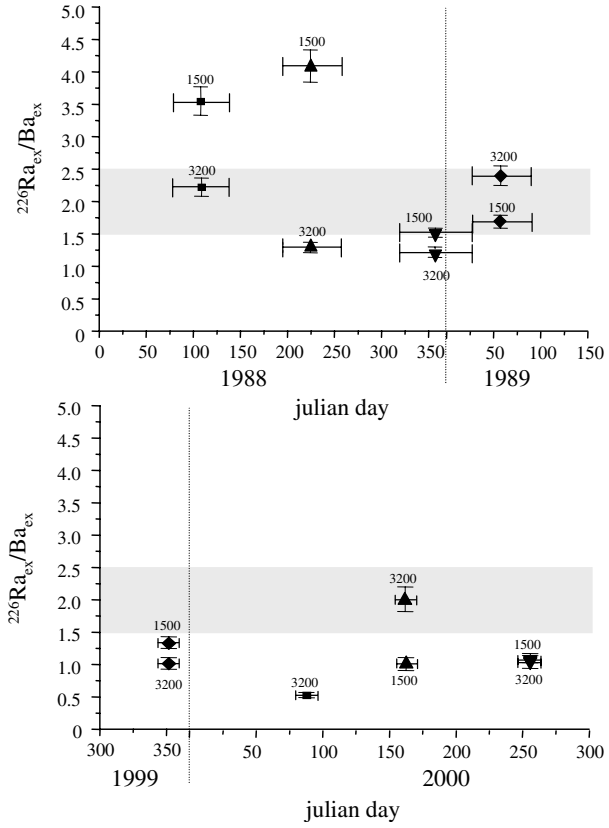

Fig. 7. $^{226}Ra_{ex}/Ba_{ex}$ ratios in sinking particles reported versus time. The depth of the sediment trap is shown on the plots. Legend is same as Fig. 6. The shaded area represents the range of values found in seawater (Fig. 5). Width of the plots indicates sampling duration.

the $^{228}Ra_{ex}/^{226}Ra_{ex}$ of suspended and sinking particles can provide some clarification on the relative importance of these various processes.

4.1.1. $^{228}Ra_{ex}/^{226}Ra_{ex}$ ratio in suspended particles

When precipitating, barite incorporates radium isotopes from seawater at the depth of formation. Because the $^{228}Ra/^{226}Ra$ ratio in seawater displays a strong vertical gradient (Fig. 4), the $^{228}Ra/^{226}Ra$ ratio of barite can be used to constrain the depth range of barite formation (Legeleux and Reyss, 1996). Barite forming in the upper water column should have higher $^{228}Ra/^{226}Ra$ ratios than barite produced in deeper water. Partial dissolution of settling barite crystals in undersaturated waters is unlikely to affect the $^{228}Ra/^{226}Ra$ ratios of barite crystals.

In the upper 500 m, the $^{228}Ra_{ex}/^{226}Ra_{ex}$ ratios in suspended particles are high (0.22–0.35 dpm/100 kg) and are close to the seawater ratio given for the same water depth (Fig. 4). This pattern agrees with the idea that barite crystals form in the upper water column, as was reported by previous studies (Dehairs et al., 1980, 1990, 1991; Bishop, 1988; Legeleux and Reyss, 1996) and as was suggested by the higher excess Ba concentrations found in this work in the upper 500 m. Deeper in the water column, the $^{228}Ra_{ex}/^{226}Ra_{ex}$ of suspended particles rapidly decreases to zero below 1000 m.

Suspended particles settle to the seafloor via cycles of aggregation and disaggregation. They sink rapidly (>100 m/day) when incorporated into large sinking particles, and very slowly when released by disaggregation. Their mean sinking rates (300–1000 m/year) have been estimated from measurements of the ^{230}Th in fine suspended particles (Krishnaswami et al., 1981; Bacon and Anderson, 1982; Bacon et al., 1985). If all the suspended Ba_{ex} found in deep water were produced in surface water with a $^{228}Ra/^{226}Ra$ of 0.38, we could predict their $^{228}Ra_{ex}/^{226}Ra_{ex}$ depth profile for a given sinking rate S (Fig. 8):

$$\left[^{228}Ra_{ex}/^{226}Ra_{ex}\right]_z = \left[^{228}Ra_{ex}/^{226}Ra_{ex}\right]_0 \exp(-\lambda_{228}\, z/S). \quad (5)$$

We also plotted the predicted $^{228}Ra_{ex}/^{226}Ra_{ex}$ depth profile of suspended particles considering that suspended Ba_{ex} was produced at ~250 m with a ratio of 0.30 because it has often been proposed that barite predominantly formed in subsurface (Dehairs et al., 1980, 1990, 1992; Stroobants et al., 1991; Legeleux and Reyss, 1996). Fitting the particulate $^{228}Ra_{ex}/^{226}Ra_{ex}$ data requires a mean sinking velocity of 40 m/year, which is well below the range of values estimated from particulate ^{230}Th. This observation implies that Ba_{ex} must also be produced in deeper water with lower initial $^{228}Ra_{ex}/^{226}Ra_{ex}$ ratios. In addition, since the $^{228}Ra_{ex}/^{226}Ra_{ex}$ of suspended particles is very close (within error bars) to the seawater ratios (Fig. 4), our data suggest very little contribution from aged barite crystals originating from the surface. Transformation during settling may potentially affect the initial $^{228}Ra/^{226}Ra$ ratio incorporated by barite in upper waters: recrystallization at depth would thus decrease the $^{228}Ra/^{226}Ra$ ratio of settling barite. However, because recrystallization would take place on existing crystals (originating from upper waters), one would expect to find only slight decreases in the $^{228}Ra/^{226}Ra$ ratio of settling barite with increasing water depth. In contrast, the $^{228}Ra_{ex}/^{226}Ra_{ex}$ activity ratios of suspended particles display a large decrease (i.e., from 0.3 to 0.4 in upper waters to <0.05 in intermediate waters). Such a large decrease could be explained by transformation only if the $^{228}Ra/^{226}Ra$ signature recorded in upper waters is (almost) entirely replaced by a $^{228}Ra/^{226}Ra$ signature recorded deeper in the water column. This scenario would imply significant (i) dissolution of barite formed in surface/subsurface waters and (ii) recrystallization below 500 m, which does not seem too consistent with the recrystallization process (i.e., recrystallisation on existing barite crystals). Therefore, it cannot be excluded that recrystallization contributes to decrease the initial $^{228}Ra/^{226}Ra$ ratio of settling barite but it is unlikely to explain the entire decrease found in suspended particles.

We can predict the $^{228}Ra_{ex}$ activity profile of suspended particles if all Ba_{ex} was produced in situ (i.e., at the depth of sample collection) from the measured $^{226}Ra_{ex}$ activities and the $^{228}Ra/^{226}Ra$ ratios of seawater (Fig. 8):

$$^{\text{Predicted}}\left[^{228}Ra_{ex}\right]_z = {}^{\text{Measured}}\left[^{226}Ra_{ex}\right]_z \times {}^{\text{Seawater}}\left(^{228}Ra/^{226}Ra\right)_z. \quad (6)$$

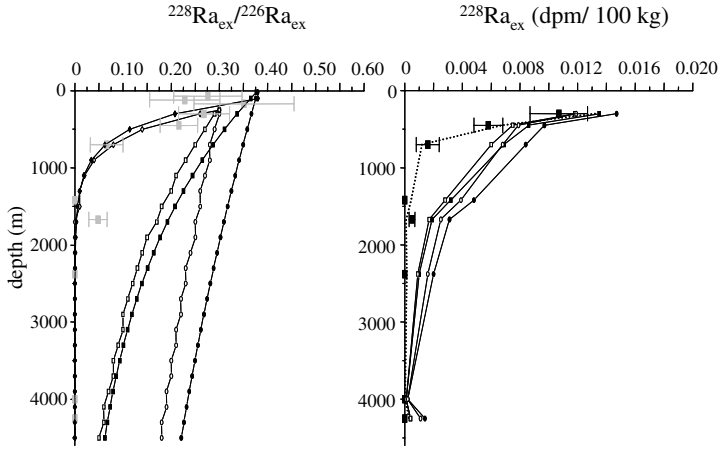

Fig. 8. (Left panel) $^{228}Ra_{ex}/^{226}Ra_{ex}$ ratio expected in suspended particles considering that the particles acquire the seawater ratio of surface waters (solid symbols; initial ratio of 0.38) or subsurface (open symbols; initial ratio of 0.30) and that they settle at a rate of 1000 m/year (circles), 300 m/year (squares) or 40 m/year (diamonds). Ratios measured in the suspended particles are shown in grey with their associated error bars. (Right panel) $^{228}Ra_{ex}$ activities expected in suspended particles collected below 250 m as deduced from the $^{226}Ra_{ex}$ activities measured in each sample and considering that the particles acquired the seawater $^{228}Ra/^{226}Ra$ ratio in surface waters (solid symbols; initial ratio of 0.38) or subsurface (open symbols; initial ratio of 0.30); Vertical profiles were computed considering settling rates of 300 m/year (squares) and 1000 m/year (circles). The dotted line represents the expected values in case Ba_{ex} incorporates the seawater ratio throughout the water column. $^{228}Ra_{ex}$ activities measured in suspended particles are also reported (solid squares with error bars).

Similarly, we can predict $^{228}Ra_{ex}$ activity profile if all Ba_{ex} was produced in surface water or subsurface and sinking at rates S ranging from 300 to 1000 m/year.

$$^{\text{Predicted}}\left[^{228}\text{Ra}_{\text{ex}}\right]_z = {}^{\text{Measured}}\left[^{226}\text{Ra}_{\text{ex}}\right]_z \times {}^{\text{Seawater}}\left(^{228}\text{Ra}/^{226}\text{Ra}\right)_0 \times \exp(-\lambda_{228}\, z/S). \quad (7)$$

$^{\text{Seawater}}(^{228}Ra/^{226}Ra)_0$ was considered to be 0.38 for surface waters and 0.30 for subsurface waters.

The predictions based on in situ production fall within the error bars of the data (Fig. 8), confirming that most of the Ba_{ex} in suspension at depth between 450 and 2380 m is produced in situ. At 4000 m and below, within the nepheloid layer, all suspended Ba can be accounted for by lithogenic material (Fig. 3). These samples appear to be significantly depleted in ^{228}Ra (i.e., ^{228}Ra activity is lower than ^{232}Th activity in the same samples), suggesting rapid loss of ^{228}Ra from resuspended sediment to the water column.

Lateral transport of old sediment resuspended from continental margins to the ocean interior, as suggested by Moore and Dymond (1991) in the Pacific Ocean, could also explain the low $^{228}Ra_{ex}/^{226}Ra_{ex}$ of suspended particles, but such lateral input would also result in higher suspended ^{232}Th concentration. The latter is relatively constant in the upper 2380 m, showing a significant increase only close to the bottom (Fig. 3; Table 2). The low $^{228}Ra_{ex}/^{226}Ra_{ex}$ ratios observed between 500 and 2000 m, therefore, are unlikely to be explained by the lateral transport of particles resuspended at the continental margins.

4.1.2. $^{228}Ra_{ex}/^{226}Ra_{ex}$ ratio in sinking particles

In most cases, the $^{228}Ra_{ex}/^{226}Ra_{ex}$ ratios found in sinking particles at 1500 and 3200 m are intermediate between that of barite (or particulate Ba_{ex}) originating from surface or subsurface waters (0.23–0.35) and those formed in deeper water (<0.1; Fig. 6). These intermediate values suggest that a significant fraction of the barite intercepted by the sediment traps originates from the upper water column, as suggested by Legeleux and Reyss (1996), but with equally significant contributions from deeper waters. The low $^{228}Ra/^{226}Ra$ ratios found in suspended particles at intermediate depths suggested that barite could form below 500 m, presumably in remaining saturated microenvironments. Such crystals may then be incorporated in the sinking flux. Recrystallization at depth may not be completely excluded and could also contribute to lower the $^{228}Ra/^{226}Ra$ ratio of sinking barite.

Barite crystals originating from upper waters, which are not found in the pool of suspended particles below 500 m, may thus either dissolve in undersaturated waters or be removed from the upper 500 m with the downward flux of large particles through aggregation processes. Considering that there is little evidence of barite release from disaggregation of large particles below 500 m (which would increase $^{228}Ra_{ex}/^{226}Ra_{ex}$ ratios of suspended particles to values higher than seawater ratios), it would appear that exchange of Ba_{ex} between the two pools of particles occurs mainly in one direction, i.e., large sinking particles entrain barite produced in deeper water but release little barite to seawater during settling. This suggests that the increase in seawater concentration in Ba and ^{226}Ra concentration is mainly due to vertical diffusion after dissolution on the seafloor, since dissolution of barite during the short residence time of large particles in the water column is unlikely to be significant.

There is a relatively large temporal and depth variability in the $^{228}Ra_{ex}/^{226}Ra_{ex}$ ratios of the sinking particles.

Legeleux and Reyss (1996) also reported significant fluctuations with time and water depth in the $^{228}Ra_{ex}/^{226}Ra_{ex}$ atio of sinking particles collected in the tropical northeast Atlantic (ratios ranging from 0.09 to 0.25 at the oligotrophic site and from 0.09 to 0.30 at the mesotrophic site). Such variability suggests significant temporal variations in the relative proportion of barite originating from surface and intermediate waters, but no pattern could be distinguished which would provide insight into what controls this variability. Mass fluxes and Ba_{ex} fluxes display large variations throughout the year (Table 3; Conte et al., 2001), but no significant correlation could be identified between the $^{228}Ra_{ex}/^{226}Ra_{ex}$ ratio of sinking particles and any of the downward fluxes (total, organic carbon, silica, carbonates, Ba_{ex}). This may in part be due to the large uncertainties in the ^{228}Ra measurements.

On occasion, $^{228}Ra_{ex}$ activity of settling particles drops below detection limits. In particular, this was observed in the sample collected in winter 1988–1989 and in three of the four samples collected during brief (2 weeks) periods in 2000 (Table 3; Fig. 6). In such instances, the intercepted Ba_{ex} could only originate from water deeper than 1000 m, with very little contribution of Ba_{ex} from surface/subsurface waters. Similarly, the addition of barite crystals precipitated below 1500 m to the downward flux could explain the decrease in the $^{228}Ra_{ex}/^{226}Ra_{ex}$ ratio of sinking particles often observed between 1500 and 3200 m.

4.2. $^{226}Ra/Ba$ ratios

The study of $^{226}Ra_{ex}/Ba_{ex}$ ratios and Sr contents can be used to reinforce our deductions based on $^{228}Ra/^{226}Ra$ data and to provide additional information on the possible role of acantharians in barite formation (Bernstein et al., 1987, 1992, 1998).

4.2.1. $^{226}Ra/Ba$ ratio in seawater

Earlier studies have indicated that the dissolved $^{226}Ra/Ba$ ratios in open ocean waters is generally uniform (2.3 dpm μmol^{-1}; Chan et al., 1976; Foster et al., 2004). The dissolved $^{226}Ra/Ba$ ratios below 500 m agree with this observation, but we find significantly lower values in the upper 500 m of the water column, above the main thermocline (Fig. 5). Similar $^{226}Ra/Ba$ profiles have been found at (old) Hale Aloha station off Hawaii and Station K3 in the North-West Pacific (van Beek et al., unpublished data), indicating that this is not a feature unique to the OFP site, and suggesting preferential uptake of Ra over Ba in the upper water column. At similar depths, salinity-normalized Sr concentrations in the Sargasso Sea reported small variations but no clear depletion in surface water which could indicate acantharians production (Mackenzie, 1964; Bernstein et al., 1992, 1998).

4.2.2. $^{226}Ra_{ex}/Ba_{ex}$ ratio in suspended particles

In the upper 500 m, fractionation during the formation of suspended particulate Ba is corroborated by the high $^{226}Ra_{ex}/Ba_{ex}$ ratios of suspended particles compared to seawater at the same depth (Fig. 5). A depth-by-depth correlation between seawater and suspended particles ratios is not warranted because of the different integration times inherent in the data sets: the seawater ratio reflects a longer-term integration whereas the ratio in suspended particles reflects a "snapshot" view. Nonetheless, $^{226}Ra_{ex}/Ba_{ex}$ ratios are clearly higher than 2.3 dpm μmol^{-1} in suspended particles collected in the upper 170 m, reaching a maximum (3.8 dpm μmol^{-1}) at 120 m depth. At the same water depth, a maximum in the non-carbonate Sr contents is observed (Fig. 5).

To a first approximation, suspended Ba_{ex} concentrations determined in this work were attributed to barite. Bernstein et al. (1992, 1998), however, suggested that acantharian skeletons made of celestite ($SrSO_4$) could play a significant role in the Ba and Ra cycle. Michaels (1988), Michaels et al. (1995) and Bernstein et al. (1992, 1998) reported the presence of abundant acantharian population in the Sargasso Sea. In the present study, we relate the high non-carbonate Sr concentrations in surface waters to acantharian skeletons. Our Sr data agree with the view that acantharians are generally concentrated in surface waters and that their abundance rapidly decreases below 150 m because celestite rapidly dissolves after the death of the organism (Bishop et al., 1977, 1978; Michaels, 1988; Michaels et al., 1995; Bernstein et al., 1992).

The highest $^{226}Ra_{ex}/Ba_{ex}$ ratio reported at 120 m that corresponds to the maximum in the non-carbonate Sr is likely to be explained by acantharian celestite (Fig. 5). Chemical analogues of strontium, both barium and radium are incorporated into celestite. Based on the solubility products of Ra, Ba and Sr sulfate at 20 °C and zero ionic strength, Bernstein et al. (1998) predicted radium enrichments in celestite. The relatively high $^{226}Ra_{ex}/Ba_{ex}$ ratios and Sr contents in the suspended particles from surface waters therefore likely indicate the presence of acantharians, and their decrease with depth must reflect the dissolution of celestite. We note, however, that even in the non-carbonate Sr maximum (120–170 m), molar Ba_{ex}/Sr_{ex} ratios remain high (0.6–0.9). This is much higher than the molar Ba/Sr ratio reported for acantharian-derived celestite (3×10^{-3}; Bernstein et al., 1992). This suggests that particles that carry Ba and Sr at such depths consist in a mixing of acantharians (high Sr content) and barite (high Ba content, which increases the Ba/Sr ratio in the suspended particles). In addition, because celestite dissolves rapidly, sampling of acantharians using in situ pumps is unlikely to be quantitative, which would lower the Sr content determined in the suspended particles. These results suggest that the dissolution of acantharian celestite in upper waters is likely to contribute significantly to barite formation. The resulting barite crystals are expected to incorporate significant amount of Sr, which would increase their solubility. Sr-enriched barite crystals that derive from acantharian celestite in upper waters may thus be more sensitive to dissolution compared with barite

crystals that were shown to precipitate deeper in the water column.

In the absence of acantharians below 500 m in suspended particles, Ba_{ex} concentrations can be more confidently attributed to barite. In these deeper waters, the $^{226}Ra_{ex}/Ba_{ex}$ ratios of suspended particle are lower than those of seawater (Fig. 5) and drop below 2.3 dpm μmol^{-1}, reaching zero at 4000 m before increasing sharply near the seafloor. Moore and Dymond (1991) also found $^{226}Ra_{ex}/Ba_{ex}$ ratios lower than 2.3 dpm μmol^{-1} in sinking particles from deep Pacific water, which they attributed to presence of old barite crystals (with a low $^{226}Ra/Ba$ ratio) from resuspended margin or deep-sea sediments. Considering the low $^{228}Ra_{ex}/^{226}Ra_{ex}$ ratios and ^{232}Th activities in the suspended particles at OFP, we concluded that barite formed in situ and were not laterally transported. Particulate ratio lower than seawater ratio would imply a preferential uptake of Ba over Ra during barite precipitation. In the upper 500 m, a similar fractionation would occur during barite precipitation, but this process would occur in microenvironments enriched in ^{226}Ra by the dissolution of celestite, thereby raising the $^{226}Ra_{ex}/Ba_{ex}$ ratio of particulate Ba (or barite) to values equal or higher to that of ambient seawater. In the nepheloid layer, Ba_{ex}, Ra_{ex} and Sr_{ex} are small compared to their lithogenic fractions and uncertainties in the lithogenic corrections prevent us to use the excess ratios in a meaningful way.

4.2.3. $^{226}Ra_{ex}/Ba_{ex}$ ratio in sinking particles

As for $^{228}Ra_{ex}/^{226}Ra_{ex}$, the $^{226}Ra_{ex}/Ba_{ex}$ ratios of sinking particles are intermediate between the ratios measured in shallow and deeper water, confirming the mixed origin of barite or Ba_{ex} intercepted by sediment traps. $^{226}Ra_{ex}/Ba_{ex}$ ratios also display significant variability with time and water depth (0.53–4.09 dpm μmol^{-1}). With smaller error bars, we can better distinguish the origin of Ba_{ex} in different seasons and years. During the 1988–1989 collection period, the Ba_{ex} intercepted at 1500 m clearly had a predominantly shallow signature (high $^{226}Ra_{ex}/Ba_{ex}$) during Spring and Summer, which is consistent with the $^{228}Ra_{ex}/^{226}Ra_{ex}$ ratios of the same samples when considering the error bars on the latter. On the other hand, the winter samples had a predominantly deep signature. It is not possible, however, to tell from this study whether the two highest $^{226}Ra_{ex}/Ba_{ex}$ values >3.5 dpm μmol^{-1} are associated with (i) barite crystals enriched in ^{226}Ra potentially deriving from the dissolution of acantharians or (ii) acantharian specimens and/or acantharian-derived particles. We note that the highest $^{226}Ra_{ex}/Ba_{ex}$ values are not associated with the highest Sr flux intercepted by the sediment traps (data not shown), as would be expected if the high ratios are associated with acantharian specimen. In addition, observations of Bernstein et al. (1992) in the Sargasso Sea concluded that acantharian specimen were rare to non-existent at 1500 m depth. However, we agree that this is non-conclusive.

In the deep trap, the $^{226}Ra_{ex}/Ba_{ex}$ ratios can more confidently be associated with barite as acantharians are not recovered at such depth (Bernstein et al., 1992). At 3200 m, the Spring and Summer samples had lower ratios than at 1500 m, suggesting addition of barite produced below 1500 m to the vertical flux. During the 1999–2000 collection period, the ratio of most sediment trap samples suggest a predominantly deep origin, as was also suggested by the $^{228}Ra_{ex}/^{226}Ra_{ex}$ ratios. In addition, the $^{226}Ra_{ex}/Ba_{ex}$ ratios lower than the seawater ratio suggest fractionation between Ra and Ba during barite precipitation, a pattern that was also deduced from the ratios of suspended particles. Consequently, ratios found at 3200 m during the two sampling periods suggest that barite (or Ba_{ex}) accumulates at the sea-floor with a $^{226}Ra/Ba$ ratio slightly lower than 2.3 dpm μmol^{-1} (i.e., mean ratio at 3200 m is 1.5 dpm μmol^{-1}).

5. Conclusion

Combining measurements of Ba_{ex}, Sr_{ex}, $^{226}Ra_{ex}$ and $^{228}Ra_{ex}$ in suspended and sinking particles and comparing their $^{228}Ra_{ex}/^{226}Ra_{ex}$ and $^{226}Ra_{ex}/Ba_{ex}$ ratios to those of seawater provide constraints on the origin and mode of formation of particulate Ba_{ex} (mostly barite) in the ocean.

1. $^{228}Ra_{ex}/^{226}Ra_{ex}$ ratios of sinking particles suggest that barite exported to the deep sea has a mixed origin that varies with season. While particles settling to a depth of 1500 m in Spring and Summer can sometimes (but not always) have barite that is predominantly formed in shallow water, in agreement with Legeleux and Reyss (1996), barite found in winter samples appear to have been produced in deeper water. At 3200 m, settling particles have generally a larger proportion of barite produced in deep water. Barite production, therefore, is not restricted to shallow water but also seems to be significant at greater depth. The mechanism postulated by Ganeshram et al. (2003), which invokes uptake of Ba by phytoplankton (with a surface Ra isotopic signature) and subsequent release in microenvironments of sinking particles, would produce a clear surface signal in the barite collected throughout the water column. Our data indicate that this proposed mechanism cannot be the only one that produces barite in the water column. Deeper in the water column, barite must also be produced within microenvironments, which must act as a sink for seawater Ba.
2. The $^{228}Ra_{ex}/^{226}Ra_{ex}$ ratios of suspended particles track closely that of seawater, confirming in situ formation of barite in deep water and minimal addition of barite by disaggregation of large sinking particles originating from the overlying mixed layer. The exchange of Ba_{ex} between suspended and sinking particles thus appear to mainly occur through the incorporation of barite produced in deep water into the settling flux.
3. The $^{226}Ra_{ex}/Ba_{ex}$ ratio of suspended particles is higher than that of seawater above 200 m and lower below 700 m. Suspended particles in the upper water column

have also high Sr content indicating the presence of celestite from acantharians. Taken together, these observations suggest (i) significant contribution of celestite dissolution to barite formation in the upper 500 m (ii) preferential precipitation of Ba over Ra during barite formation.

4. Regarding implications for paleoceanographic studies, the results reported here indicate that (i) the relationship between barite and productivity is more complex than previously thought (i.e., barite can precipitate deeper than 500 m depth; celestite dissolution may contribute significantly to barite precipitation) and (ii) the elemental and isotopic composition of seawater recorded by barite that accumulates in deep-sea sediments cannot be strictly related to a seawater pattern from the upper 500 m of the water column.

Acknowledgments

We are grateful to the crew and captain of Weatherbird II. We thank Christophe Monnin for the calculation of the Ba saturation index at the OFP site. The manuscript was significantly improved by constructive reviews by three anonymous reviewers and Kelly Falkner, associate editor. We thank Larry Ball and David Schneider at the ICP/MS of WHOI, USA; Valérie Olive at the ICP/MS of East Kilbride, Scotland, UK; Frédéric Candaudap at the ICP/MS of Observatoire Midi Pyrénées, Toulouse; Carole Causserand at the atomic spectrophotometry, Observatoire Midi Pyrénées, Toulouse. We are grateful to John C. Weber for his help with the sinking particles samples. We also thank Alan Fleer, Susan Brown-Léger and Bernhard Peucker-Ehrenbrink at WHOI. We thank Charlotte Riccio, Thierry Zampieri and Jean-Louis Saury at the underground laboratory of Modane as well as Sophie Ayrault, Serge Boiziau at the Laboratoire Pierre Süe, Saclay. We are grateful to Paul Lethaby and Christine Pequignet (BBSR) for providing the CTD data. This work was supported by a Lavoisier fellowship given by the French Ministry of Foreign Affairs and by the Woods Hole Oceanographic Institution.

Associate editor: Kelly K. Falkner

References

Anderson, R.F., Lao, Y., Broecker, W.S., Trumbore, S.E., Hofman, H.J., Wolfli, W., 1990. Boundary scavenging in the Pacific Ocean: a comparison of ^{10}Be and ^{231}Pa. *Earth Planet. Sci. Lett.* **96**, 287–304.

Bacon, M.P., Anderson, R.F., 1982. Distribution of thorium isotopes between dissolved and particulate forms in the deep sea. *J. Geophys. Res.* **87**, 2045–2056.

Bacon, M.P., Edmond, J.M., 1972. Barium at GEOSECS III in the Southwest Pacific. *Earth Planet. Sci. Lett.* **16**, 66–74.

Bacon, M.P., Huh, C.-A., Fleer, A.P., Deuser, W.G., 1985. Seasonality in the flux of natural radionuclides and plutonium in the deep Sargasso Sea. *Deep-Sea Res. I* **32** (3), 273–286.

Berkman, P.A., Ku, T.-L., 1998. $^{226}Ra/Ba$ ratios for dating Holocene biogenic carbonates in the Southern Ocean: preliminary evidence from Antarctic coastal mollusc shells. *Chem. Geol.* **144**, 331–334.

Bernstein, R.E., Byrne, R.H., 2004. Acantharians and marine barite. *Mar. Chem.* **86**, 45–50.

Bernstein, R.E., Betzer, P.R., Feely, R.A., Byrne, R.H., Lamb, M.F., Michaels, A.F., 1987. Acantharian fluxes and strontium to chlorinity ratios in the North Pacific Ocean. *Science* **237**, 1490–1494.

Bernstein, R.E., Byrne, R.H., Betzer, P.R., Greco, A.M., 1992. Morphologies and transformations of celestite in seawater: the role of acantharians in strontium and barium geochemistry. *Geochim. Cosmochim. Acta* **56**, 3273–3279.

Bernstein, R.E., Byrne, R.H., Schijf, J., 1998. Acantharians: a missing link in the oceanic biogeochemistry of barium. *Deep-Sea Res. II* **45**, 491–505.

Bishop, J.K.B., 1988. The barite–opal–organic carbon association in oceanic particulate matter. *Nature* **332**, 341–343.

Bishop, J.K.B., Edmond, J.M., Ketten, D.R., Bacon, M.P., Silker, W.B., 1977. The chemistry, biology, and vertical flux of particulate matter from the upper 400 m of the equatorial Atlantic Ocean. *Deep-Sea Res.* **24**, 511–548.

Bishop, J.K.B., Ketten, D.R., Edmond, J.M., 1978. The chemistry, biology, and vertical flux of particulate matter from the upper 400 m of the Cape Basin in the southeast Atlantic Ocean. *Deep-Sea Res.* **25**, 1121–1161.

Broecker, W.S., Li, Y.H., Cromwell, J., 1967. Radium-226 and Radon-222: concentration in Atlantic and Pacific Oceans. *Science* **158**, 1307–1310.

Broecker, W.S., Goddard, J., Sarmiento, J.L., 1976. The distribution of ^{226}Ra in the Atlantic Ocean. *Earth Planet. Sci. Lett.* **32**, 220–235.

Chan, L.H., Edmond, J.M., Stallard, R.F., Broecker, W.S., Chung, Y.C., Weiss, R.F., Ku, T.L., 1976. Radium and barium at GEOSECS stations in the Atlantic and Pacific. *Earth Planet. Sci. Lett.* **32**, 258–267.

Chan, L.H., Drummond, D., Edmond, J.M., Grant, B., 1977. On the barium data from the Atlantic GEOSECS expedition. *Deep-Sea Res.* **24**, 613–649.

Chow, T.J., Goldberg, E.D., 1960. On the marine geochemistry of barium. *Geochim. Cosmochim. Acta* **20**, 192–198.

Chung, Y.-C., 1974. Radium-226 and Ra–Ba relationships in Antarctic and Pacific waters. *Earth Planet. Sci. Lett.* **23**, 125–135.

Chung, Y.-C., 1976. A deep ^{226}Ra maximum in the northeast Pacific. *Earth Planet. Sci. Lett.* **32**, 249–257.

Chung, Y.-C., Craig, H., 1980. ^{226}Ra in the Pacific Ocean. *Earth Planet. Sci. Lett.* **49**, 267–292.

Church, T.M., Wolgemuth, K., 1972. Marine barite saturation. *Earth Planet. Sci. Lett.* **15**, 35–44.

Conte, M.H., Ralph, N., Ross, E.H., 2001. Seasonal and interannual variability in deep ocean particles fluxes at the Oceanic Flux Program (OFP)/Bermuda Atlantic Time Series (BATS) site in the western Sargasso Sea near Bermuda. *Deep-Sea Res.* **48**, 1471–1505.

Dehairs, F., Chesselet, R., Jedwab, J., 1980. Discrete suspended particles of barite and the barium cycle in the open ocean. *Earth Planet. Sci. Lett.* **49**, 528–550.

Dehairs, F., Goeyens, L., Stroobants, N., Bernard, P., Goyet, C., Poisson, A., Chesselet, R., 1990. On suspended barite and the oxygen minimum in the Southern Ocean. *Global Biogeochem. Cycles* **4** (1), 85–102.

Dehairs, F., Stroobants, N., Goeyens, L., 1991. Suspended barite as tracer of biological activity in the Southern Ocean. *Mar. Chem.* **35**, 399–410.

Dehairs, F., Baeyens, W., Goeyens, L., 1992. Accumulation of suspended barite at mesopelagic depths and export production in the Southern Ocean. *Science* **258**, 1332–1335.

Dickey, T., Zedler, S., Frye, D., Jannasch, H., Manov, D., Sigurdson, D., McNeil, J.D., Dobeck, L., Yu, X., Gilboy, T., Bravo, C., Doney, S.C., Siegel, D.A., Nelson, N., 2001. Physical and biogeochemical variability from hours to years at the Bermuda Testbed Mooring site: June 1994–March 1998. *Deep-Sea Res. II* **48**, 2105–2140.

Dymond, J., Suess, E., Lyle, M., 1992. Barium in deep-sea sediment: a geochemical proxy for paleoproductivity. *Paleoceanography* **7** (2), 163–181.

Foster, D.A., Staubwasser, M., Henderson, G.M., 2004. ^{226}Ra and Ba concentrations in the Ross Sea measured with multicollector ICP mass spectrometry. *Mar. Chem.* **87**, 59–71.

François, R., Honjo, S., Manganini, S.J., Ravizza, G.E., 1995. Biogenic barium fluxes to the deep sea: implications for paleoproductivity reconstruction. *Global Biogeochem. Cycles* **9** (2), 289–303.

Ganeshram, R.S., François, R., Commeau, J., Brown-Leger, S.L., 2003. An experimental investigation of barite formation in seawater. *Geochim. Cosmochim. Acta* **67** (14), 2599–2605.

Gingele, F., Dahmke, A., 1994. Discrete barite particles and barium as tracers of paleoproductivity in South Atlantic sediments. *Paleoceanography* **9** (1), 151–168.

Jacquet, S.H.M., Dehairs, F., Rintoul, S., 2004. A high resolution transect of dissolved barium in the Southern Ocean. *Geophys. Res. Lett.* **31**, L14301. doi:10.1029/2004GL020016.

Joyce, T.M., Robbins, P., 1996. The long-term hydrographic record at Bermuda. *J. Climate* **9**, 3121–3131.

Kaufman, A., Trier, R.M., Broecker, W.S., Feely, H.W., 1973. Distribution of ^{228}Ra in the world ocean. *J. Geophys. Res.* **78** (36), 8827–8848.

Kim, G., Hussein, N., Church, T., 2003. Tracing the advection of organic carbon into the subsurface Sargasso Sea using ^{228}Ra/^{226}Ra tracer. *Geophys. Res. Lett.* **30** (16), 1874. doi:10.1029/2003GL017565.

Krishnaswami, S., Sarin, M.M., Somayajulu, B.L.K., 1981. Chemical and radiochemical investigations of surface and deep particles in the Indian Ocean. *Earth Planet. Sci. Lett.* **54**, 81–96.

Ku, T.-L., Lin, M.-C., 1976. ^{226}Ra distribution in the Antarctic Ocean. *Earth Planet. Sci. Lett.* **32**, 236–248.

Ku, T.-L., Huh, C.-A., Chen, P.S., 1980. Meridional distribution of ^{226}Ra in the eastern Pacific along GEOSECS cruise tracks. *Earth Planet. Sci. Lett.* **49**, 293–308.

Legeleux, F., Reyss, J.-L., 1996. Ra-228/Ra-226 activity ratio in oceanic settling particles: Implications regarding the use of barium as a proxy for paleoproductivity reconstruction. *Deep-Sea Res. I* **43** (11–12), 1857–1863.

Li, Y.H., Ku, T.L., Mathieu, G.G., Wolgemuth, K., 1973. Barium in the Antarctic Ocean and implications regarding the marine Geochemistry of Ba and ^{226}Ra. *Earth Planet. Sci. Lett.* **19**, 352–358.

Li, Y.H., Feely, H.W., Toggweiler, J.R., 1980. ^{228}Ra and ^{228}Th concentrations in GEOSECS Atlantic surface waters. *Deep-Sea Res.* **27A**, 545–555.

Mackenzie, F.T., 1964. Strontium content and variable strontium-chlorinity relationship of Sargasso Sea water. *Science* **146**, 517–518.

Michaels, A.F., 1988. Vertical distribution and abundance of Acantharia and their symbionts. *Mar. Biol.* **97**, 559–569.

Michaels, A.F., Caron, D.A., Swanberg, N.R., Howse, F.A., Michaels, C., 1995. Planktonic sarcodines (Acantharia, Radiolaria, Foraminifera) in surface waters near Bermuda: abundance, biomass and vertical flux. *J. Plankton Res.* **17** (1), 131–163.

Monnin, C., Cividini, D., 2006. The saturation state of the world's ocean with (Ba,Sr)SO_4 solid solutions. *Geochim. Cosmochim. Acta* **70**, 3290–3298.

Monnin, C., Jeandel, C., Cattaldo, T., Dehairs, F., 1999. The marine barite saturation state of the world's oceans. *Mar. Chem.* **65**, 253–261.

Moore, W.S., 1987. Radium 228 in the South Atlantic Bight. *J. Geophys. Res.* **92**, 5177–5190.

Moore, W.S., Dymond, J., 1991. Fluxes of Ra-226 and barium in the Pacific Ocean: the importance of boundary processes. *Earth Planet. Sci. Lett.* **107**, 55–68.

Moore, W.S., Reid, D.F., 1973. Extraction of radium from natural waters using manganese-impregnated acrylic fibers. *J. Geophys. Res.* **78**, 8880–8886.

Moore, W.S., Key, R.M., Sarmiento, J.L., 1985. Techniques for precise mapping of 226Ra and 228Ra in the ocean. *J. Geophys. Res.* **90**, 6983–6995.

Nürnberg, C.C., Bohrmann, G., Schlüter, M., 1997. Barium accumulation in the Atlantic sector of the Southern Ocean: results from 190,000-year records. *Paleoceanography* **12** (4), 594–603.

Paytan, A., Kastner, M., Chavez, F.P., 1996a. Glacial to Interglacial fluctuations in productivity in the equatorial Pacific as indicated by marine barite. *Science* **274**, 1355–1357.

Paytan, A., Moore, W.S., Kastner, M., 1996b. Sedimentation rate as determined by ^{226}Ra activity in marine barite. *Geochim. Cosmochim. Acta* **60** (22), 4313–4319.

Reyss, J.-L., Schmidt, S., Legeleux, F., Bonte, P., 1995. Large, low background well-type detectors for measurements of environmental radioactivity. *Nucl. Instrum. Methods A* **357**, 391–397.

Rhein, M., Schlitzer, R., 1988. Radium-226 and barium sources in the deep East Atlantic. *Deep-Sea Res.* **35** (9), 1499–1510.

Rushdi, A., McManus, J., Collier, R., 2000. Marine barite and celestite saturation in seawater. *Mar. Chem.* **69**, 19–31.

Schmitz, B., 1987. Barium, equatorial high productivity, and the northward wandering of the Indian continent. *Paleoceanography* **2** (1), 63–77.

Sherrell, R.M., Boyle, E.A., 1992. The trace metal composition of suspended particles in the oceanic water column near Bermuda. *Earth Planet. Sci. Lett.* **111**, 155–174.

Stroobants, N., Dehairs, F., Goeyens, L., Vanderheijden, N., van Grieken, R., 1991. Barite formation in the Southern Ocean water column. *Mar. Chem.* **35**, 411–421.

Staubwasser, M., Henderson, G.M., Berkman, P.A., Hall, B.L., 2004. Ba, Ra, Th, and U in marine mollusc shells and the potential of 226Ra/Ba dating of Holocene marine carbonate shells. *Geochim. Cosmochim. Acta* **68** (1), 89–100.

Steinberg, D.K., Carlson, C.A., Bates, N.R., Johnson, R.J., Michaels, A.F., Knap, A.H., 2001. Overview of the U.S. JGOFS Bermuda Atlantic Time-Series Study (BATS): a decade look at ocean biology and biogeochemistry. *Deep-Sea Res.* **48**, 1405–1448.

Talley, L., 1996. North Atlantic circulation and variability, reviewed for the CNLS conference. *Physica D*, 625–646.

Taylor, S.R., McLennan, S.M., 1985. *The Continental Crust: Its Composition and Evolution*. Blackwell, Cambridge, MA.

van Beek, P., Reyss, J.-L., 2001. ^{226}Ra in marine barite: new constraints on supported ^{226}Ra. *Earth Planet. Sci. Lett.* **187**, 147–161.

van Beek, P., Reyss, J.-L., Gersonde, R., Paterne, M., Rutgers van der Loeff, M., Kuhn, G., 2002. ^{226}Ra in barite: absolute dating of Holocene Southern Ocean sediments and reconstruction of sea-surface reservoir ages. *Geology* **30** (8), 731–734.

van Beek, P., Reyss, J-L., DeMaster, D., Paterne, M., 2004. ^{226}Ra-in marine barite: relationship with carbonate dissolution and sediment focusing in the equatorial Pacific. *Deep-Sea Res. I* **51**, 235–261.

Wolgemuth, K., Broecker, W.S., 1970. Barium in sea water. *Earth Planet. Sci. Lett.* **8**, 372–378.